Three-Dimensional Shock Wave Distortion in Shock-Square Vortex Loop Interaction

Takahiro Ukai*, Hossein Zare-Behtash, Konstantinos Kontis

School of Engineering, University of Glasgow, Scotland G12 8QQ, UK

Shigeru Obayashi

Institute of Fluid Science, Tohoku University, 2-1-1 Katahira, Aoba-ku, Sendai, Miyagi, 980-8577, Japan

Corresponding author:** ***Takahiro Ukai

email: Takahiro.Ukai@glasgow.ac.uk

Telephone and Fax: + 44-141-330-2477

Abstract:

Understanding of the three-dimensional shock wave-vortex loop interaction phenomena plays a key role in noise reduction. This study focuses on the three-dimensional shock wave distortion and propagation phenomena in a near-field supersonic jet. Shock-square vortex loop interaction was experimentally investigated in a square cross-sectional open-end shock wave generating tube at an incident shock Mach number of 1.39 ± 0.05. A square vortex loop impinged on a reflected shock wave from a wall located in front of the nozzle end. The planar reflected shock wave transforms into either a concave or convex distorted shape due to the opposing high-speed flow emitted from the nozzle corner. The convex shaped shock wave scatters towards the outside of the vortex loop, whereas the concave one converges towards the centre of the vortex loop. The concave shaped shock wave results in shock wave focusing. In shock-square vortex loop interaction, the shock wave is locally focused along the axis of the nozzle corner.

Keywords:

Shock wave interaction; square vortex loop; shock wave focusing

1. Introduction

Compressible vortex loops are mainly generated by shock wave emission through a tube into a quiescent fluid. Their flow features are strongly related to the nozzle geometry of the tube. After an incident shock wave is emitted from the nozzle exit, the shock wave diffraction generated at the nozzle corner induces an initial circulation which develops into a vortex. The angle of the nozzle corner is an important factor in vortex circulation [1-3]. Sun *et al*. [3] numerically conducted vorticity prediction in shock diffraction at various corner angles and showed that the vorticity production dramatically increases in the range of 15 to 45 degrees; however, it hardly increases at corner angles over 90 degrees and reaches a constant value. When three-dimensional fluid motion is taken into account, shock wave diffraction leads to the generation of a vortex loop. Circular vortex loops that produce fundamental three-dimensional fluid motion are frequently addressed in vortex loops studies [4-7]. The main features of vortex loops are that they are self-contained, automotive, and quite longevous [8]. Different exit nozzle geometries, which are non-circular in shape, change the flow characteristics and induce unsteady and highly three-dimensional flows. Zare-Betash *et al.* [9, 10] reported the flow features of non-circular vortex loops from various nozzle geometries such as the square, elliptic, and exotic shapes. The PIV results of Zare-Betash *et al.* [10] indicated that the circulation of a circular vortex loop is higher than that of a non-circular one because the deceleration of some parts of the non-circular vortex loop induce a relatively lower circulation. According to the numerical simulation of Zhang *et al.* [11], a square vortex loop leads to counter-rotating stream-wise vortices at the four corners, and they accelerate mixing in the vortex core because they engulf the surrounding air into the vortex core. Therefore, the nozzle geometry is a key parameter influencing flow characteristics such as velocity and vorticity of a vortex loop, and various nozzle shapes are used for various engineering applications.

Rectangular supersonic jets have the ability to enhance mixing, reduce jet noise, and be applied for the thrust vector control [12]. Additionally, rectangular supersonic jets are useful for a wide range of applications such as combustion, noise suppression, heat transfer, and lift augmentation. According to previous investigations, where various nozzle geometries have been evaluated for jet noise reduction in high-subsonic and supersonic flows [13], a circular nozzle produces a higher level of jet noise, whereas a rectangular nozzle has a higher performance for noise reduction. Additionally, rectangular jets that play a key role in noise generation and jet plume impingement govern the performance of the vectored thrust on aircrafts. Screech tones, relating to jet noise generation, may also have a detrimental effect on aircraft structures. Raman [14] showed that the level of screech tones altered depending on a span-wise nozzle exit geometry. Rectangular jets have also been used for combustors [15, 16] and they

lead to enhancement of the combustion performance due to axis switching associated with self-induced vortex ring deformations.

Shock waves generated in supersonic jets are often accompanied by induced vortex rings [17-19], and there is a high possibility that these flows interact with each other, which results in noise generation. Understanding shock-vortex loop interaction phenomena are important for noise detection/reduction in high speed flows [20-22] and the automobile exhaust flow fields [23-25]. Since the early 1990s, there have been experimental, numerical, and theoretical investigations of shock wave interaction with vortex rings [20-22, 26, 27]. Minota [28] experimentally investigated shock-vortex ring interactions when the shock wave impinges head-on. She showed that the diffracted shock wave which interacts with the vortex ring propagates towards the centre of the vortex ring, which results in the shock wave focusing at the centre of the vortex ring. This shock focusing causes a pressure increase that would lead to noise generation [29, 30]. According to a numerical investigation by Meadows [31], the sound pressure level increases with increasing shock wave strength, and this relation was consistent with previous experimental observations in supersonic jets.

Understanding of shock wave interaction with three-dimensional vortex loop is also a key issue for noise generation. Shimizu *et al.* [22] experimentally and theoretically investigated the mechanism of noise generation in shock-vortex ring interaction in a three-dimensional flow field. They focused on investigating noise generation at the early stage of the interaction. Noise generation comes from the scattered waves involving the shock diffraction, the acoustic wave, and the backward scattering by density inhomogeneity. Inoue *et al.* [32] numerically investigated sound generation in a long interaction process and showed large sound pressures occur due to shock wave focusing. Shock wave focusing in shock-vortex ring interaction had also been observed computationally by Takayama *et al.* [29]. Therefore, shock wave deformations such as diffraction, reflection, and focusing may lead to enhanced noise generation. Since non-circler vortex loops have self-induced vortex deformation, it leads to a more complicated mechanism for sound generation. This study focuses on investigating three-dimensional shock wave distortion and propagation phenomena. An experimental investigation of shock-square vortex loop interaction was conducted at an incident shock Mach number of 1.39 in a square cross-sectional open-end shock wave generating tube. The high-speed shadowgraph photography technique was used to evaluate flow characteristics.

2. Experimental setup

An experimental investigation was conducted in a square cross-sectional open-end shock wave generating tube at an incident shock Mach number of 1.39 ± 0.05 in the driven section with a Reynolds

number of 7.2×10^5 based on a side length of the tube. The shock wave generating tube with side lengths of d = 22 mm consists of a driven section of 200 mm in length and a blasted section (Fig. 1). The wall thickness of the tube is 1.2 mm. A flush-mounted pressure transducer (Kulite Semiconductor Products, Inc., model: XTE-190M, natural frequency: 150 kHz) was positioned 50 mm from the exit of the tube, and the Mach number in the driven section is estimated from the measured overpressure magnitude. The pressure signal was recorded using a data acquisition (National Instruments Corp., model: NI-9205, sampling rate: 250 kS/s, resolution: 16 bit) driven by LabVIEW. A non-electric tube (Dyno Nobel, model: NONEL DynoLine) was used to induce a shock wave which propagates into the driven section. The shock wave generating system using the NONEL tube has been successfully applied in a previous study [33]. The flexible NONEL tube with an outer diameter of 3 mm was flush mounted on the shock generating tube end in the blasted section, and the axis of the NONEL tube was aligned with the shock propagation direction. The detonation was initiated within the NONEL tube by an electric blasting device (Dyno Nobel, model: Dyno Start 2, output voltage: 2500 V). This explosion generates a blast wave from the NONEL tube end, and the blast wave transforms into a planar shock wave in the driven section. NONEL tube of 300 mm in length was used for each run.

After the planar incident shock is emitted from the nozzle exit, a vortex loop is generated behind it, and its shape transforms with time (Fig. 2). The incident shock wave is reflected from a wall located in front of the nozzle exit, and this reflected shock wave impinges on the vortex loop. The distance between the wall and the shock generating tube was L = 55 mm. The velocity of the reflected shock wave just before vortex impingement was 317.6 ± 18.9 m/s which is a Mach number of less than 1.0. Shock-induced opposing flow might cause the reduction in the shock wave propagation speed.

High-speed shadowgraph photography with a standard Z-type optical arrangement was employed to visualise the flow density field. The shadowgraph system consists of a 450 to 1000 W continuous light source with an Xe-Hg arc lamp (Newport, model: 66921), a pair of 203.3 mm diameter concave mirrors with a focal length of 1829 mm, and a high-speed camera (Photron, model: Fastcam SA1.1). The images were acquired at a frame rate of 72 kfps with an exposure time of 1.0 μs. The offset angle between the collimated light beam and the light source was set to 19 degrees to prevent coma.

3. Results and discussion

Shadowgraph photography captures self-induced unsteady vortex motion, which enables us to understand the three-dimensional flow characteristics. Figure 3 shows the time evolution shadowgraph images of the three-dimensional vortex loop without shock interaction. The upper and lower rows show the 0 and 45 degrees rotation side views, respectively. These views help to visualise three-

dimensional vortex motion from different perspectives. The elapsed time after shock wave emission from the nozzle is defined as t. To evaluate the characteristics of vortex loop motion independently, the wall located in front of the shock generating tube was removed. The strong density change of areas (1) and (2), observed in the 0 degree rotation side view (Fig. 3 (b)), corresponds with that of the 45 degrees rotation side view (Fig. 3 (h)). The mean outer diameter of the vortex core was 1.4 ± 0.4 mm. The images [(b), (h)], [(c), (i)], and [(d), (j)] were similar to the shape in Fig. 2 (I), (II), and (III), respectively; this is identical to previous studies [10, 11]. The shape of the vortex loop alters and reconstructs to the original shape with expansion and contraction. The vortex loop possessing a concave shape (Fig. 3 (b)) becomes the similar concave shape again (Fig. 3 (f)) after the transformation, although the outer diameter of the vortex D_v is different.

Figures 4 and 5 show the time evolution of vortex motion and the instantaneous velocity of the upper vortex core. The velocity coordinate for positive or negative signs is defined in Fig. 3 (a). u and v denote the instantaneous horizontal and vertical velocities, respectively. The semi-transparent grey areas correspond to the timing of shock-vortex loop interaction. At the region of shock-vortex loop interaction, although the instantaneous vertical velocities measured on the 0 and 45 degrees rotation side views slightly alter (Fig. 5), vertical vortex loop motion is almost constant at the interaction region (Fig. 4). In the 0 degree rotation side view (see Fig. 4, the circle symbols), the outer diameter tends to increase over time but dramatically reduces at approximately t = 360 μs. At approximately t = 300 μs, the vortex loop becomes the square shape as in Fig. 2 (III), and then the corners of the square vortex loop move towards its centre. This is because the instantaneous vertical velocity of the vortex core dramatically increases at t = 360 μs (see v in Fig. 5 (a)) as well as the instantaneous vertical velocity in the 45 degrees view (Fig. 5 (b)). At approximately t = 400 μs in the 45 degrees rotation side view, a high vertical velocity leads to a sudden vortex movement, and then the shape of the vortex loop becomes similar to the shape of the originally emitted vortex loop.

The time evolution of the intensity of the density gradient provides the opportunity for a deeper understanding of the shock interaction phenomena. Figures 6 and 7 show the time evolved shadowgraph images of shock-vortex loop interaction, as well as the intensity profiles of the density gradient obtained along the semi-transparent white line displayed in the shadowgraph images. The intensity of the density gradient is averaged based on the obtained value from the line width of 1.1 mm. The position of the white line corresponds to the nozzle centre line. The intensity of the density gradient was normalised by the brightness of the image background so that the unchanged magnitude can be subtracted from the images. The lateral axis denotes the normalised distance x/d from the nozzle end. Note the high intensity of the density gradient implies a steep density gradient.

As shown in previous studies [19, 28], the shock wave interaction process is divided into two sections: the outer and the central parts of the vortex ring. In shock wave interactions with square vortex loops, the behaviour generating the retarded/diffracted shock waves at the outer and central parts of the vortex loop resembles that of interaction with a circular vortex loop. Before the reflected shock wave (RSW) impinges on the vortex loop (VL), the shape of the RSW is almost planar (Figs. 6 and 7, image (1)). The RSW passing through the central part of the VL is obstructed by the opposed flow induced by the vortex (Figs. 6 and 7, image (2)). At the outer portions of the VL, the RSW is accelerated by the rotating vortex core, which results in the generation in a diffracted shock wave (DSW) (see Figs. 6 and 7, image (4)). The DSW converges towards the centre of the VL. In the case of interacting with a circular vortex loop, the planar shaped RSW is deformed to become the concave shape at the central portion due to the rotating vortex core [28-30], whereas the planar shaped RSW does not necessarily transfer to the concave shape, in the case of interacting with the present square vortex loop.

The local high-speed flow emitted from the square nozzle corner induces a strong distortion of the shock wave interacting with the VL. In the 0 degree rotation side view (Fig. 6, image (3)), the distorted shock wave around the outer vortex core is affected by the high-speed flow at the vortex corner (C in image (3)). According to a previous study that the velocity field was measured in front of a square nozzle [10], the high-speed flow occurs along the axis of the square nozzle corner. The high-speed flow reduces the shock propagation velocity at the vortex corner (C in image (3)), and the shock wave is distorted towards the centre of the VL. Thereafter, the distorted shock wave impinges on the outer vortex core. When the RSW interacts with the outer vortex core, the outer vortex core moves forward at approximately 100 m/s. This movement of the outer vortex core pulls the distorted shock wave and leads to the scattering of the shock wave towards the outer portion (Fig. 6, image (6)). Around the centre of the VL, the almost planar RSW transforms to a convex shape as shown in the image (5), and then propagates towards the outside of the VL. In contrast, in the 45 degrees rotation side view (see Fig. 7), as mentioned regarding the opposing high-speed flow effect, the RSW at the outer vortex core is strongly distorted towards the centre of the VL (Fig. 7, image (3)). The almost planar RSW becomes the concave shape at the central portion due to the opposing high-speed flow (Fig. 7, image (4)), and it converges towards the centre line. Different shock distortions observed between the 0 and 45 degrees rotation side views enable us to deduce the three-dimensional shock propagation.

The shape of the distorted shock wave governs the wave propagation direction and influences the shock wave focusing phenomena. As shown on the graphs in Figs 6 and 7, the RSW impinges on the VL which slowly moves from left to right. The peak intensity of the density gradient of the RSW

gradually reduces with time before the shock-vortex loop interaction. In three-dimensional shock wave propagation, its overpressure magnitude decreases non-linearly, and it causes the reduction in peak intensity of the density gradient of the RSW. However, when the RSW impinges on the VL, the peak intensity of the density gradient is intensified because of the strong density change induced by the shock-vortex loop interaction (Figs. 6 and 7, graphs (4)). Then, this peak intensity gradually decreases again due to the non-linear effects. On the other hand, for the 45 degrees rotation side view (Fig. 7), the peak intensity of the distorted shock wave is intensified again (see Fig. 7, graph (7)). This is because the concave shaped shock wave generated at the central portion converges towards the centre line, which results in a shock wave focusing phenomenon. The shock waves are strongly focused along the axis of the nozzle corner due to the conversion of the distorted shock wave. In the 0 degree rotation side view (Fig. 6, images (5)-(9)), the distorted shock wave scatters towards the outside of the vortex loop; thus, the shock wave does not focus at the central portion. In the case of the shock interacting with a circler vortex loop, the DSW generated from the outer vortex core focuses towards to the central torus vortex ring, and the overpressure dramatically increases [29]. In the present shock-square vortex loop interaction, the DSW is not simultaneously generated from whole of the vortex core; thus, the influence of the DSW focusing is weak in spite of the appearance of the DSW focusing.

4. Conclusion

The focus of this study is the investigation of the three-dimensional shock wave distortion and propagation phenomena in a shock-square vortex loop interaction. The experimental investigation was conducted in a square cross-sectional open-end shock generating tube at an incident shock Mach number of 1.39 ± 0.05 in the driven section, and a Reynolds number is 7.2×10^5 based on the tube side length d = 22 mm. A square vortex loop impinged on the incident shock wave reflected from a wall located L/d = 2.5 in front of the nozzle end, and its interaction behaviour was visualised using high-speed shadowgraph photography. The opposing high-speed flow emitted from the nozzle corner strongly influences the distortion of the shock wave interacting with the vortex loop. The shock wave propagation velocity was locally retarded by the opposing high-speed flow, and it caused either the concave or convex shaped distorted shock waves. The convex shaped shock wave scattered towards the outside of the vortex loop, whereas the concave one converged towards the centre of the vortex loop. As a consequence, the concave shaped shock wave led to shock wave focusing. In shock-square vortex loop interaction, the shock wave focusing does not necessarily occur at the central axis of the vortex loop; the shock wave is locally focused along the axis of the nozzle corner.

Acknowledgment

The authors are grateful to Mr. Masataka Honna, technical staff of the Institute of Fluid Science, Tohoku University for the manufacturing of the shock wave generating tube.

References

1. Skews, B.W. “The perturbed region behind a diffracting shock wave,” *J. Fluid Mech.* 29 (4), 705-719 (1967).
2. Griffith, W., Brickl, D. E., “The diffraction of strong shock waves,” *Physical Review* 89 (2), 451-453 (1953).
3. Sun, M., Takayama, K., “Vorticity production in shock diffraction,” *J. Fluid Mech.* 478, 237-256 (2003).
4. Mack, L.M., “The compressible viscous heat conducting vortex,” *J. Fluid Mech.* 8, 284-306 (1960).
5. Moore, D.W., “The effect of compressibility on the speed of propagation of a vortex ring,” *Proc. R. Soc. Lond. A* 397 (1812), 87-298 (1985).
6. Baird, J.P., “Supersonic vortex rings,” *Proc. R. Soc. Lond. A* 59-65 (1987).
7. Arakeri, J.H., Das, D., Krothapalli, A., Lourenco, L., “Vortex ring formation at the open end of a shock tube: a particle image velocimetry study,” *Physics of Fluids* 16, 1008-1019 (2004).
8. Dziedzic, M., Leutheusser, H.J., “An experimental study of viscous vortex rings,” *Exp. Fluids* 21, 315-324 (1996).
9. Zare-Behtash, H., K. Kontis, K., and Gongora-Orozco, N., “Experimental investigations of compressible vortex loops” *Phys. Fluids* 20, 126105 (2008).
10. Zare-Behtash H., Kontis K., Gongora-Orozco N., Takayama K., “Compressible vortex loops: Effect of nozzle geometry,” *Int. J. Heat Fluid Flow* 30, 561-576, (2009).
11. Zhang, H., Chen, Z., Jiang, X., Guo, Z., “The initial flow characteristics of supersonic jets with different geometries,” *Physics Letters A* 379, 1256-1262 (2015).
12. Gutmark, E.J., Grinstein, F.F., “Flow control with noncircular jets,” *Annu. Rev. Fluid Mech.* 31, 239‑272 (1999).
13. Ahuja, K., Manes, J.P., Massey, K.C., Calloway, A.B., “An evaluation of various concepts of reducing supersonic jet noise,” AIAA paper 90-3982 (1990).
14. Raman, G., “Screech tones from rectangular jets with spanwise oblique shock-cell structures,” NASA Contractor report 198417, AIAA-96-0643 (1996).
15. Gutmark, E., Schadow, K.C., Parr, T.P., Hanson-Parr, D.M., Wilson, K.J., “Noncircular jets in combustion systems,” *Exp Fluids* 7, 248-258 (1989).
16. Grinstein, F.F., Gutmark, E., Parr, T., “Near field dynamics of subsonic free square jets. A computational and experimental study,” *Phys. Fluids* 7 (6) 1483-1497 (1995).
17. An, R., Kontis, K., Edwards, J.A., “Compressible vortex-ring interaction studies with a number

of generic body configurations," *AIAA Journal* 44 (12), 2962-2978 (2006).

18. Mariani, R., Quinn, M.K., Kontis, K., Marraffa, L., "Shock-free compressible vortex rings impinging on a stationary surface: effects of surface angle variation," *Exp. Therm. Fluid Sci.* 47, 126–142, (2013).
19. Kontis, K., An, R., Zare-Behtash, H., Kounadis, D., "Head-on collision of shock wave induced vortices with solid and perforated walls," *Phys. Fluids* 20, 016104 (2008).
20. Inoue, O., Takahashi, Y., "Successive generation of sounds by shock–strong vortex interaction," *Phys. Fluids* 12 (12), 3229-3234 (2000).
21. Minota, T., Kambe, T., Murakami, T., "Acoustic emission from interaction of a vortex ring with a sphere," *Fluid Dyn. Res* 3, 357-362 (1988).
22. Shimizu, T., Watanabe, Y., Kambe, T., "Scattered waves generated by shock wave and vortex ring interaction," *Fluid Dyn. Res* 27, 65-90 (2000).
23. Kima, H.-D., Kweona, Y.-H., Setoguchi, T., "A study of the weak shock wave propagating through an engine exhaust silencer system," *J. Sound Vib.* 275, 893‑915 (2004).
24. Higashiyama, J., Iwamoto, J., "Experimental study of exhaust noise generated by pulsating flow downstream of pipe end," *JSAE Review* 20, 73-79 (1999).
25. Sekine, N., Matsumura, S., Aoki, K., Takayama, K., "Generation and propagation of shock waves in the exhaust pipe of a 4 cycle automobile engine," *AIP Conference Proceedings* 208, 671-676 (1990).
26. Tokugawa, N., Ishii, Y., Sugano, K., Takayama, F., Kambe, T., "Observation and analysis of scattering interaction between a shock wave and a vortex ring," *Fluid Dyn. Res* 21, 185-199 (1997).
27. Jiang, Z., Wang, C., Miura, Y., Takayama, K. "Three-dimensional propagation of the transmitted shock wave in a square cross-sectional chamber," *Shock Waves* 13, 103-111 (2003).
28. Minota, T., "Interaction of a shock wave with a high-speed vortex ring," *Fluid Dyn. Res* 12, 335-342 (1993).
29. Takayama, F., Ishii, Y., Sakurai, A., Kambe, T., "Self-intensification in shock wave and vortex interaction," *Fluid Dyn. Res* 12, 343-348 (1993).
30. Ding, Z., Hussaini, M.Y., Erlebacher, G., Krothapalli, A., "Computational study of shock interaction with a vortex ring," *Phys. Fluids* 13 (10), 3033-3048 (2001).
31. Meadows, K.R., "A study of fundamental shock noise mechanisms," NASA Technical Paper 3605 (1997).
32. Inoue, O., Takahashi, Y., "Successive generation of sounds by shock–strong vortex interaction,"

Phys. Fluids 12, 3229 (2000).

33. Zare-Behtash H., Gongora-Orozco N., Kontis K., Jagadeesh G., "Study of detonation interactions inside a two-dimensional ejector using detonation transmission tubing," *J. Propul. Power* 26 (4), 878-882, (2010).

Figures

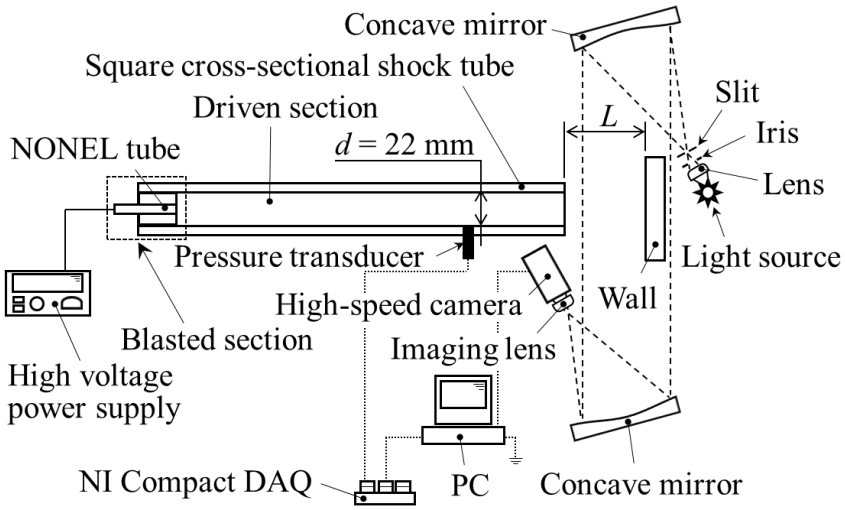

FIG. 1: Schematic of the experimental setup

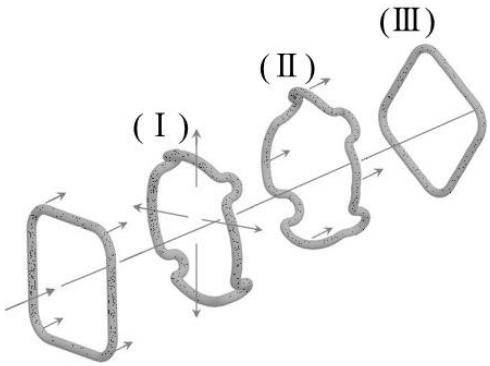

FIG. 2: Time sequential motion of the square vortex loop [10]

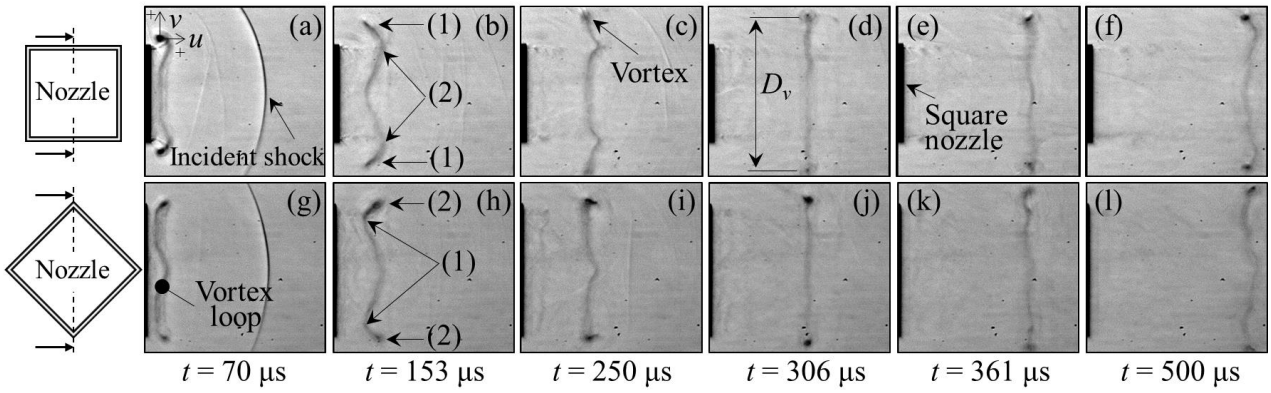

FIG. 3: A three-dimensional vortex loop without shock interaction. Framing shadowgraph images; (a-f): 0 degree rotation side view, (g-l): 45 degrees rotation side view

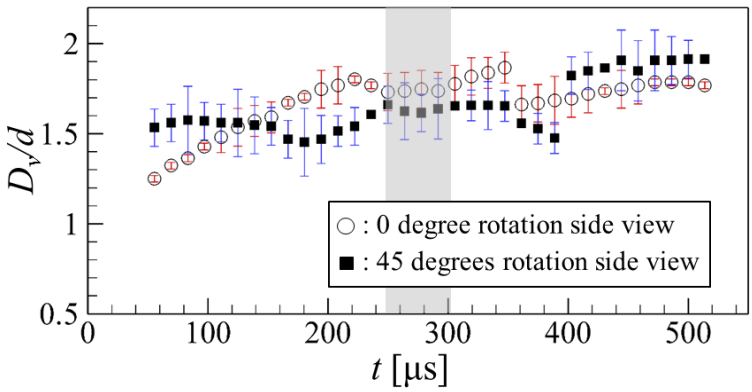

FIG. 4: Time evolution of the vortex motion

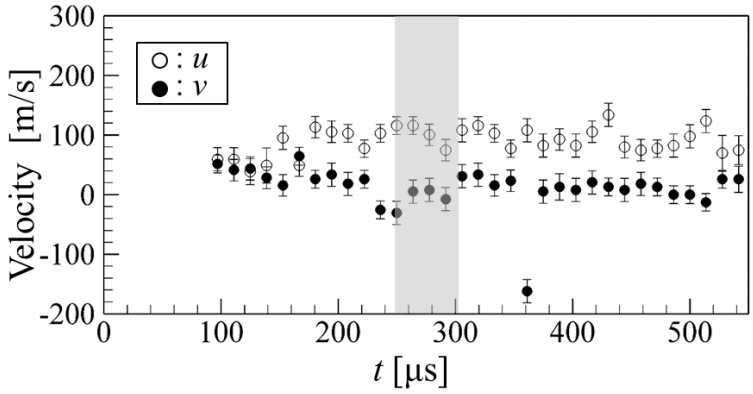

(a) Measured on 0 degree rotation side view

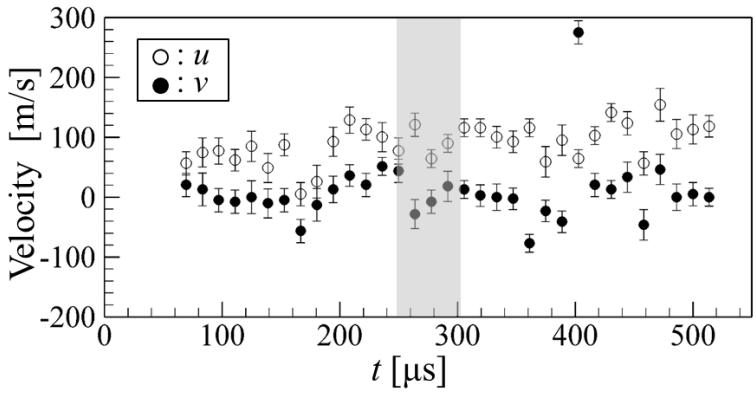

(b) Measured on the 45 degrees rotation side view

FIG. 5: Instantaneous horizontal and vertical velocities of the upper vortex core

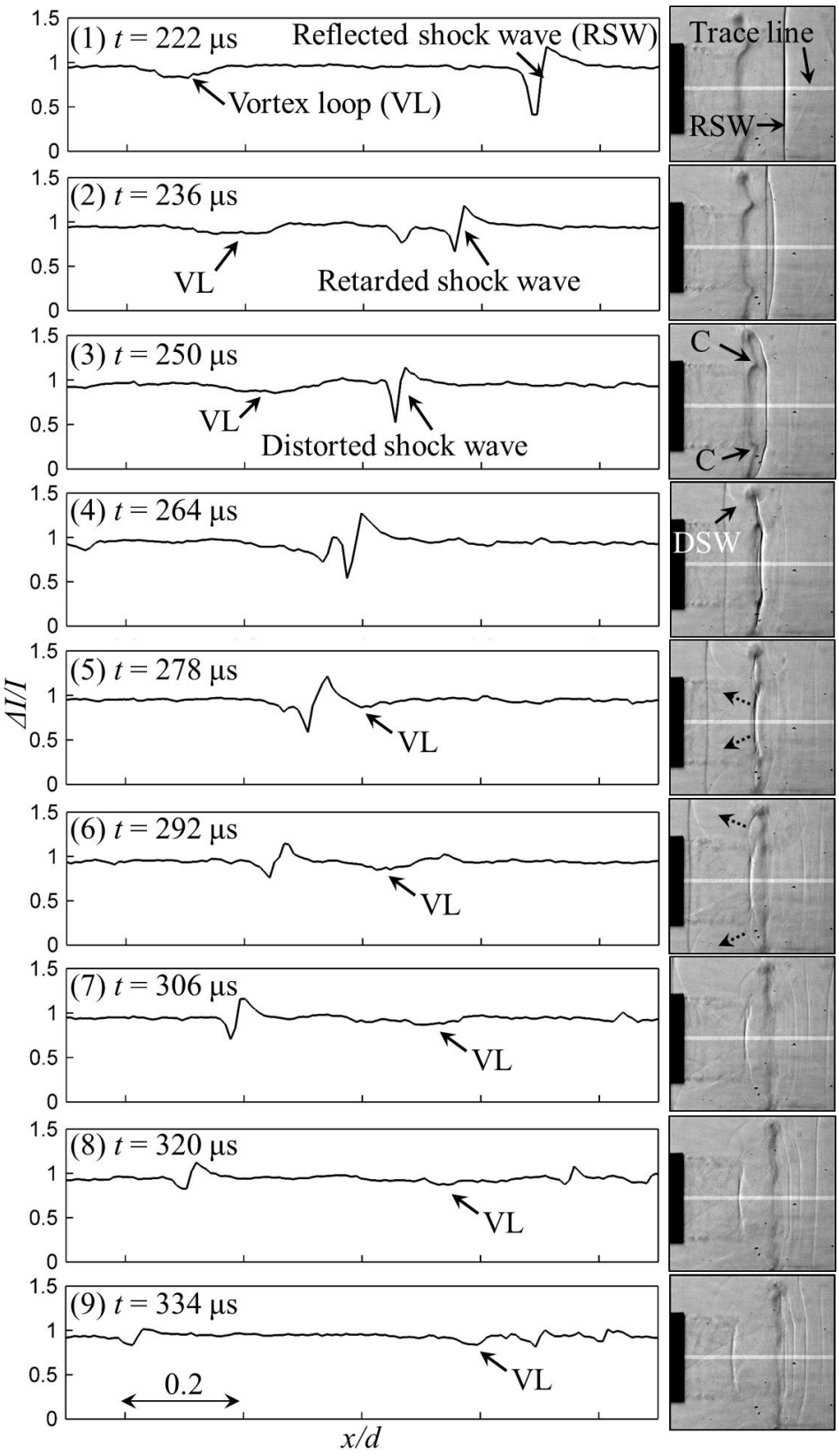

FIG. 6: Framing shadowgraph images and the intensity profile of the density gradient from line displayed in shadowgraph images, shock-vortex loop interaction case on 0 degree rotation side view

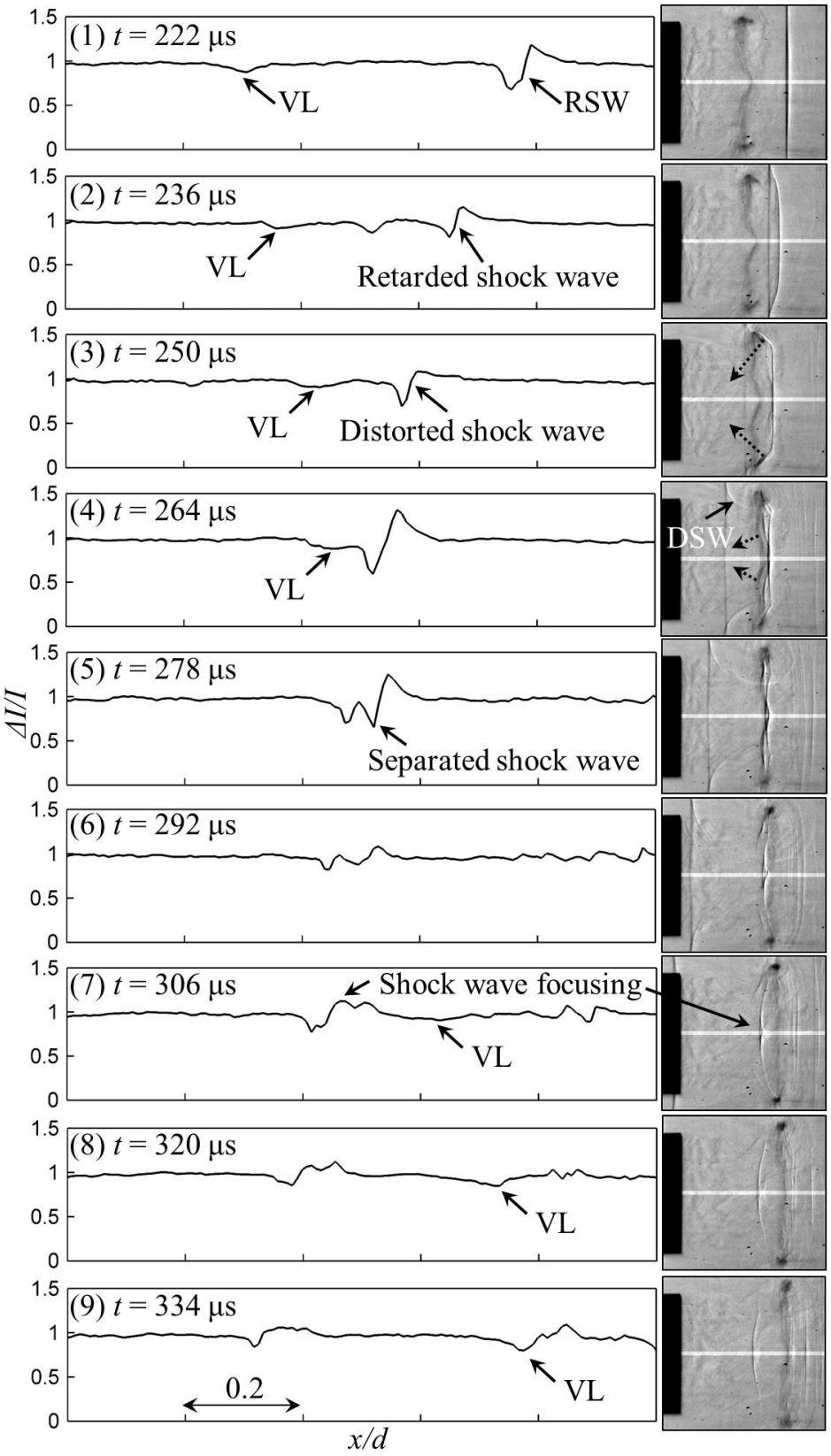

FIG. 7: Framing shadowgraph images and the intensity profile of the density gradient from line displayed in shadowgraph images, shock-vortex loop interaction case on 45 degree rotation side view